Doctoral Thesis

博士論文

Fluid segregation and chemical compaction in deep-seated rocks: A combined experimental and digital rock physics approach

深部岩石における流体分離と化学圧密：実験とデジタル岩石物理学の複合アプローチ

Wakana Fujita (藤田和果奈)

令和 4 年

Abstract

To understand the elementary processes of fluid segregation in texturally equilibrated rocks, we synthesized C–H–O fluid bering quartzite having 1.9–18.0% fluid in volume fraction and X_{CO2} = 0–0.44 at 1 GPa and 900 °C. The microstructure of the obtained run products was captured by the scanning electron microscope and synchrotron radiation X-ray computed microtomography (SRμCT). In chapter 1, we focus on the observation of the capsule-scale fluid segregation (CFS) which was identified by the heterogeneity in porosity distribution in the obtained quartzite and quartzite retaining much lower porosity (~0.3%) than added fluid fraction. Because CFS occurred irrelevantly to the expected thermal gradient in the capsule, we assumed the driving force of CFS as the pressure difference between fluid rich and poor domains invoked by the different poroelastic response under a stress change. We estimated the flux of the dissolved SiO_2 transport through thin fluid tubules along the grain edges. A porosity-evolution model was applied to the formation of the syn-metamorphic veins in schists and fluid segregation in subducting eclogite to deduce the time-scale of the poroelastic cementation. In chapter 2, we focus on the grain-scale fluid pools retained in the quartzite which was formed by grain-scale fluid segregation (GFS) during grain growth. Through the digital rock physics approach, I investigated the three-dimensional pore structure using the Pore Network Model (PNM) to show the distinct difference between CO_2-free and CO_2-bering samples. Permeability was computed by using image subvolumes obtained by SRμCT, which showed an agreement with the laboratory measurements. By analyzing the computed fluid velocity, I found a subvolume which has high permeability even at low connected porosity. By combining the experimental observation and the computed results, I discussed the effect of GFS and the specific surface area on permeability.

Chapter 1

Introduction

Aqueous fluids play an essential role in physical properties and chemical transport in the interior of the Earth. In subduction zone, for example, pore fluids left in the slab controls the volume of water down-dragged into the deep interior of the Earth in subduction zones. The fate of pore fluids is determined by the balance of efficiency between fluid segregation and matrix compaction (i.e. permeability, viscosity of solid matrix) [e.g. 1]. Recent numerical modeling of viscoelastic slabs has shown that elasticity becomes dominant when the bulk viscosity of the matrix is large and a large proportion of the fluid is trapped in the high-porosity region produced by the fluid source [2]. In this study, sintering experiments of fluid-bearing quartzite indicated almost complete sealing of pores in an undrained system. I focused on the effects of poroelasticity on cementation in the run products and applied the constructed porosity evolution model for formation of the syn-metamorphic veins in schists and fluid segregation in subducting eclogite.

Method

A mechanically mixed powder of amorphous silica synthesized by the sol-gel method and fine quartz powder (1:3 weight) was prepared as the starting material in the experiments. As a fluid source,

brucite and the oxalic acid were added to produce volumetric fluid fraction of 1.9–18.0 vol.% and three different CO_2 fractions in fluid, i.e., X_{CO2} = 0, 0.27–0.29, and 0.44–0.47 (X_{CO2}: mole fraction of CO_2). The experiments were conducted at 900 °C and 1 GPa for 24–382 h using a Boyd–England-type 3/4 inch piston-cylinder apparatus. The synchrotron radiation X-ray computed microtomography (SRμCT) was conducted at the BL20XU experimental hutch2 of SPring-8 [3] for 17 representative experimental products.

Results

Significant variation was observed in the capsule-scale homogeneity of porosity in the run products from the backscattered electron images (BSE) (Fig. 1.1) which indicates that capsule-scale fluid segregation (CFS) occurred during the experiments. The BSE and SRμCT images show that dense part of quartzite retains ~0.3% of fluid regardless of the high added fluid fraction. Because 1) CFS occurred irrelevantly to the expected thermal gradient in the capsule, 2) no signature of deformation was found from the grown quartz grains of run products and 3) grain growth occurred efficiently is samples which experienced CFS, we assumed the driving force of CFS as the pressure difference between fluid rich and poor domains invoked by poroelasticity. Fluid-rich rock is elastically “soft” (i.e. having larger Skempton’s coefficient) compared to fluid-poor rock to increase pore fluid pressure under a compressional stress change (Fig. 1.2). Therefore, more silica dissolves in fluid-rich domains with higher solubility, while it precipitates in fluid-poor domains through diffusive transport, expanding porosity contrast. This poroelastic cementation in the capsule scale is effective as long as elasticity dominates matrix viscosity because the pressure difference relaxes with time. By assuming the fluid pressure difference as 3.5–7.0 MPa and Fick’s first law of diffusion, I obtained dissolved SiO_2 flux and diffusivity as 1.1×10^{-6}–1.7×10^{-6}4 mol m^{-2} s^{-1} and 7.5×10^{-11}–1.9×10^{-10} m^2 s^{-1} respectively from the constructed a model of porosity evolution in undrained rocks. The obtained diffusion coefficient corresponds to SiO_2 diffusion in aqueous fluid through thin tubules along grain edges with porosity of 0.095–0.24%. The obtained diffusivity was interpreted as a diffusion path transition from fully interconnected fluid tubules to tightly sintered grain boundaries.

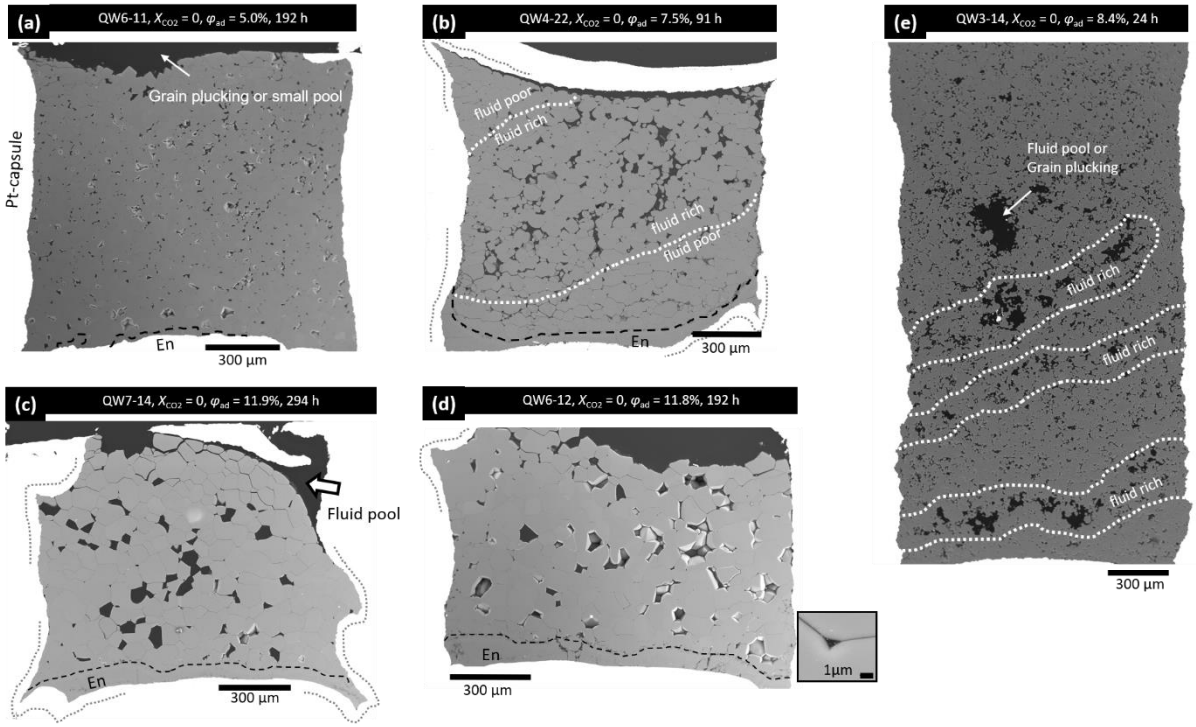

Fig. 1.1 Representative Backscattered electron (BSE) images of synthesized quartzite with fluid (X_{CO2} = 0), representing three types of fluid distribution, namely homogeneous fluid distribution (a, QW6-11), heterogeneous fluid distribution (b, QW4-22; c, QW3-14), and almost complete segregation (d, QW7-14; e, QW6-12). The retained porosity of the entire cross-sectional area of (d) and (e), and that of the low porosity parts in (b) is much smaller than is the added fluid fraction, showing that capsule-scale fluid segregation (CFS) occurs during the experiments. Only tiny pores of ~0.1–1 µm size are retained in some triple junctions of the dense part (e, inset). The grain sizes of the quartzite that experienced CFS (b, d, and e) are larger than are those of the samples not subjected to CFS. The polygonal areas inside the quartzite in (c)–(e) are not pores but plucked grains. The Pt-lined nickel capsules are subject to ductile deformation, particularly in (b), (d), and (e) (grey dotted lines), where particularly dense quartzites are formed. Below the dashed lines at the bottom of the samples in (a, b, d, and e) is the enstatite layer formed by the reaction between the added brucite and quartz. Scale bars are 300 µm in (a)–(e) and 10 µm in the inset of (e).

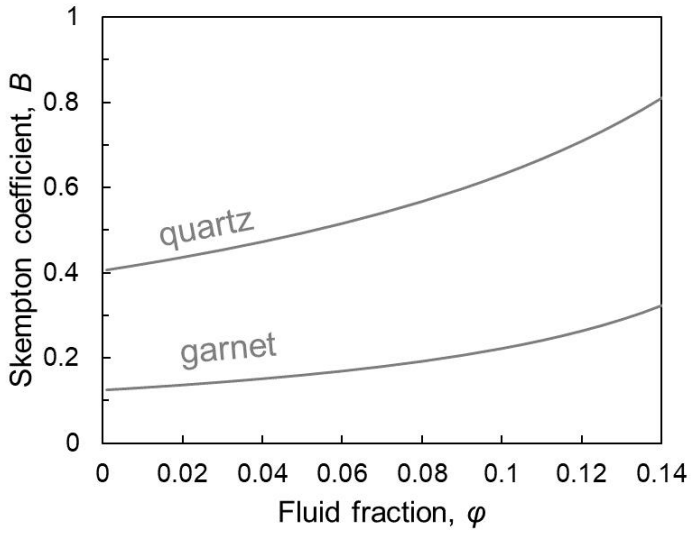

Fig. 1.2. Skemptons's coefficient ***B*** of aqueous fluid-bearing quartzite and garnetite as a function of fluid fraction, ***φ***.

Discussion

The poroelastic cementation model was applied to the formation of syn-metamorphic vein and subducting rocks by calculating the Skempton's coefficient of quartzite and garnetite. The time-scale for which the pressure difference invoked by poroelasticity can be maintained was calculated as the relaxation time of viscoelastic body. The cementation mechanism found in the present experiments may explain the formation of veins with centimeter-scales within tens of thousands of years through the metamorphism of layered rocks. The poroelastic cementation may contribute to the final stage segregation of fluids retained in the pores of subducting rocks that had initial elasticity heterogeneity of less than 30–40 cm.

Chapter 2

Introduction

Diffusion-based microstructural maturation operates on a limited spatial scale, even at high temperatures and geological timescales. However, this process is crucial as a control on longer-scale fluid segregation by determining permeability. Permeability is an intrinsic rock property used to assess the efficiency of fluid segregation and is obtained in various ways such as estimation using hydrologic models based on geothermal and metamorphic data, laboratory measurements and numerical simulation. The aim of this chapter is to clarify the microstructural characteristics of fluid-expelling rocks and quantitatively describe their permeability as a function of porosity.

Method

C–H–O fluid bearing quartzites were synthesized in the same manner as described in Chapter 1.

Image subvolumes were prepared from the synchrotron radiation X-ray computed microtomography (SRμCT). Using the subvolumes, the pore structure was analyzed by Pore Network Model through SNOW algorithm [4] and permeability was computed using the finite-difference Lithospheric and Mantle Evolution Model (LaMEM) [5, 6].

Results

Based on the BSE images of the polished sections of the run products, we classified the pore fluids in the quartz aggregate into the following three types in terms of the number of surrounding grains: (1) fluid lenses, (2) triple junction tubules, and (3) fluid pools. The fluid pools were often surrounded by several to multiple grains in the two-dimensional SRμCT slices, forming irregular shapes. The sizes of the fluid pools were generally larger than those of the fluid lenses and the triple junction tubules, which were sometimes comparable to or larger than the mean grain diameter.

The distributions of pore, throat size and coordination number characterized by using Pore Network Model (PNM) approach (Fig. 2.1) show clear difference for fluid fractions (1.3–7.9%) and fluid compositions (X_{CO2} = 0–0.044).

The relationship between porosity and the computed permeability shows good agreement with the empirical model [7] but some subvolumes show lower values. However, in the relationship between the "connected porosity" and the computed permeability, the deviations from the empirical model disappeared except for one subvolume.

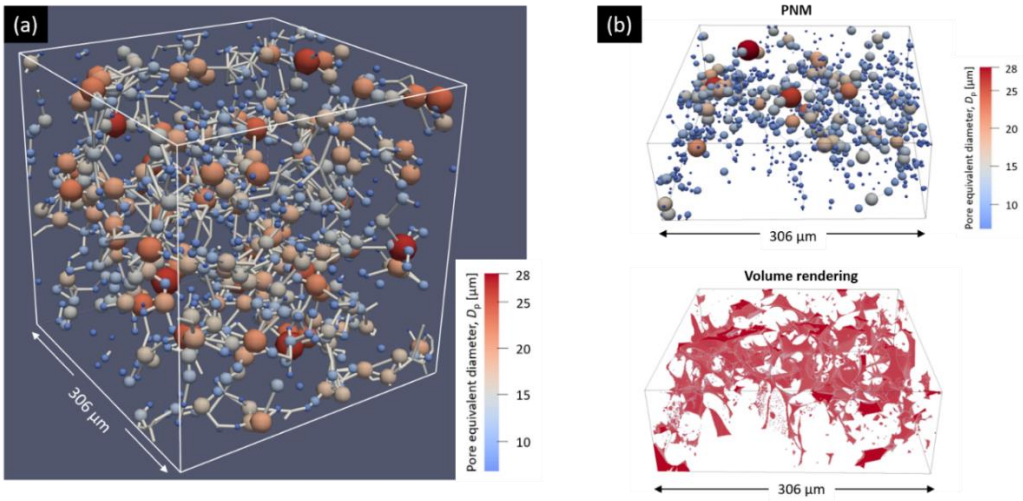

Fig. 2.1. (a) Extracted PNM structure using SNOW algorithm. Colored spheres represent the pores scaled by the pore equivalent diameter. The throat equivalent diameter is kept constant for this visualization. The pore equivalent diameter D_p ranges from 2–28 μm as shown in a color bar. The edge length of the box is 306 μm. (b) Comparison between PNM and the original volume rendering shows that spheres correspond to the large pores. The pore equivalent diameter D_p ranges from 2–28 μm as shown in a color bar. The longest edge length of the box is 306 μm.

Discussion

The obtained normalized permeabilities were lower than the theoretical value at a given porosity. This is interpreted as the effect of the reduced diameter of the triple junction tubules due to formation of fluid pools in the synthesized quartzite. The obtained normalized permeabilities nicely fit to the empirical porosity-permeability relation if the porosity is corrected to the interconnected porosity. A subvolume with the lowest φ_{mes} (1.7 vol.%) showed the exceptionally high permeability despite its very low porosity (Fig. 2.2 d). The effect of specific surface area and microstructure evolution such as grain growth and faceting on permeability is discussed.

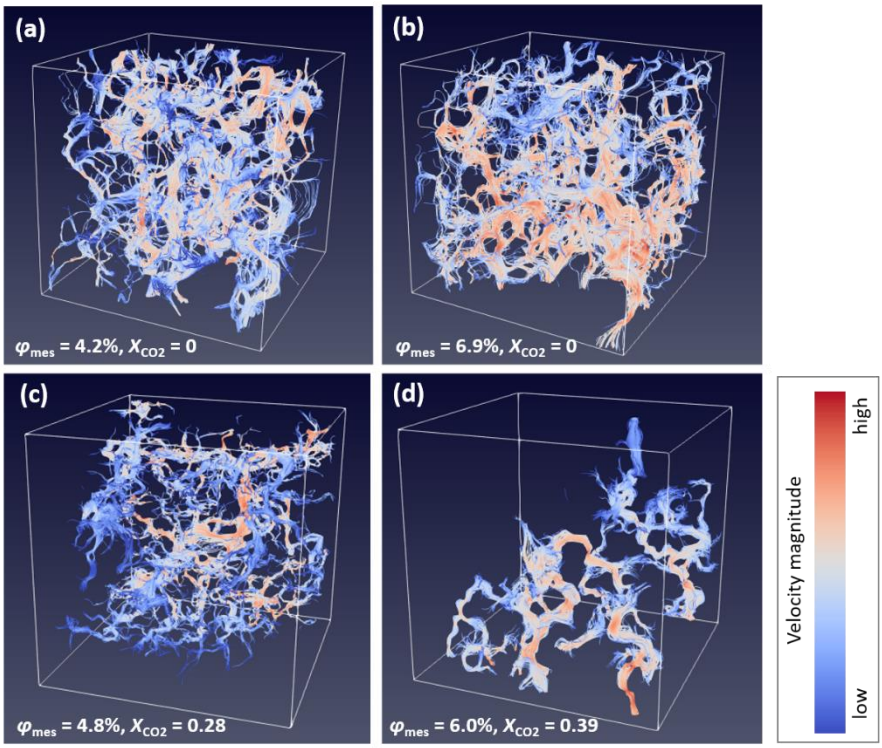

Fig. 2.2 Visualization of streamlines of the fluid velocity using an open-source application ParaView for four representative subvolumes: (a) QW13-13#2; (b) QW14-21#2; (c) QW14-11#1; (d) QW15-13#2). The high- and low- velocity channels are shown in red and blue, respectively. The high-velocity commonly distributes in thick channels, suggesting that fluids selectively flow in the wider pore spaces. A subvolume QW15-13#2 (d) shows a remarkable difference in flow patterns compared to the other three subvolumes, consisting significantly fewer channels than the others.

Reference

1. Mckenzie, D. (1984). The generation and compaction of partially molten rock. *Journal of Petrology*, 25, 713–765.

2. Morishige, M., and van Keken, P. E. (2018). Fluid Migration in a Subducting Viscoelastic Slab. Geochemistry, Geophysics, Geosystems, 19, 337–355.
3. Uesugi, K., Hoshino, M., Takeuchi, A., Suzuki, Y. and Yagi, N. (2012). Development of fast and high throughput tomography using CMOS image detector at SPring-8. *Proceedings of SPIE*, 8506.
4. Gostick, J. T. (2017). Versatile and efficient pore network extraction method using marker-based watershed segmentation. *Physical Review E*, 96.
5. Kaus, B. J. P., Popov, A. A., Baumann, T. S., Pusok, A. E., Bauville, A., Fernandez, N., and Collignon, M. (2016). Forward and Inverse Modelling of Lithospheric Deformation on Geological Timescales. *NIC Series*, 48, 978–3.
6. Eichheimer, P., Thielmann, M., Popov, A., Golabek, G. J., Fujita, W., Kottwitz, M. O., and Kaus, B. J. P. (2019). Pore-scale permeability prediction for Newtonian and non-Newtonian fluids. *Solid Earth*, 10, 1717–1731.
7. Wark, D. A., and Watson, E. B. (1998). Grain-scale permeabilities of texturally equilibrated, monomineralic rocks. *Earth and Planetary Science Letters*, 164, 591–605.